

The 27 February 2010 Maule, Chile tsunami: initial height and propagation from uniform and non-uniform fault slip models

Ergin Ulutaş*

*Department of Geophysical Engineering, Kocaeli University, Kocaeli, Turkey

[E-mail: ergin@kocaeli.edu.tr]

Received 28 January 2015 ; revised 22 August 2016

The 27 February 2010 Maule (Chile) tsunami was numerically modeled using the SWAN (Simulating WAVes Near-Shore) code which solves the non-linear long wave equations of fluid flow by a finite difference algorithm. The computational area is divided into two computational domains with a grid of 2 arc min and 0.5 arc min. Bathymetry data for the domains are interpolated from the General Bathymetry Chart of the Ocean (GEBCO) 30 arc-seconds grid data. Results from uniform and non-uniform slip models are compared with available tide gauges and Deep-ocean Assessment and Reporting of Tsunami (DART) buoy records.

[Keywords: Tsunami simulation, shallow water theory, finite fault model, slip distribution]

Introduction

A massive earthquake (M_w 8.8) struck Chile on 27 February, 2010. The earthquake was the sixth largest instrumentally recorded earthquake in history and the largest in the region after the earthquake of 22 May 1960 with a magnitude of 9.5. Epicenter was located at 72.733° W, 35.909° S^o. Earthquake occurred at a depth of 35 km¹ on the subduction zone named Andean-type, sometimes termed Chilean-type². This type considered to have a shallow plate dip and a very high degree of intraplate coupling whereas the Marianas type³ is thought to have a steep plate dip and low coupling². The subduction in Chile is very active and the seismicity of the Chilean subduction zone presents many striking features³. It is known that Chile has been struck by destructive earthquakes^{4,5,6,7,8} and the great earthquake record shows a remarkably well defined cyclicity^{9,10}. The main ruptures of the earthquakes in Chile dominate subduction zone convergence and regional crustal deformation¹¹. Subduction occurs at the Peru–Chile Trench where the Nazca oceanic plate descends beneath a convergent continental margin of the South America plate at a rate of approximately 80

mm/year^{2,12,13}. The contact between these two plates is also the source of accompanying tsunamis with very large earthquakes, depths ranging between 15 and 50 km, known as interplate, thrust events^{13,14,15}. Coastal and offshore earthquakes of magnitude greater than 7.5 normally generate severe tsunamis along the Chilean coast depending on the shape and geometry of the bays³. Massive earthquake and accompanying tsunami of Maule, Chile on 27 February, 2010 is one of the great earthquakes in recorded history struck central Chile. However, the epicenter was located in a clearly identified seismic gap area within the subduction zone where no major shallow earthquakes had occurred since 1835^{16,17,18,19}. Gap had been the subject of recent seismic and geodetic investigations^{20,21}, which provide constraints on the megathrust geometry and the down-dip extent of the previously locked region²². The 2010 Chile earthquake took place in the seismic gap surrounded by the rupture areas of the M_w 9.5, 1960 earthquake in the south, the M_w , 8.0 1928 earthquake in the north, M_w 7.9, 1939 earthquake in the east (Fig. 1). The 1939 event near Chillan was an intra-slab rupture, but the others are

believed to have been on the megathrust²². Shortly after the earthquake, a destructive tsunami hit the central and south coast of Chile. More than 500 people were killed and thousands were displaced by the earthquake and tsunami. Although the majority of the fatalities are attributed to the earthquake, the tsunami accounts for 124 victims concentrated in the coastal regions of Maule (69) and Biobio (33), Juan Fernandez Archipelago's Robinson Crusoe Island (18), and Mocha Island (4)²³. Despite the large magnitude, the wide rupture area and the shallow focal depth, the earthquake generated only local destructive tsunami. On this basis, it is important not only to understand the near field effects of this tsunami, but also to simulate tsunami propagation due to source and fault models for possible future events in the region. The aim of this study is to investigate the cause of local tsunami by using a source generation approach in the shape of uniform and non-uniform slip distributions along the ruptured fault.

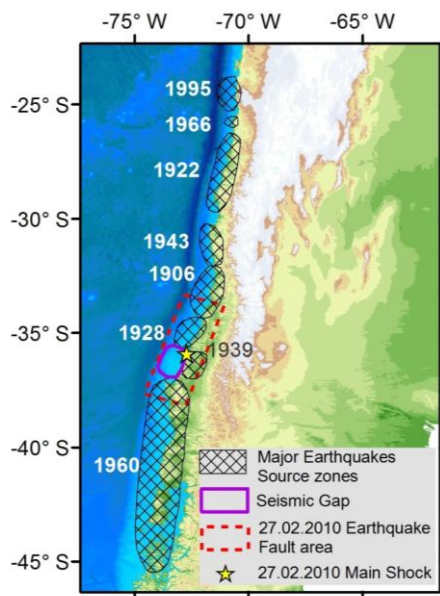


Fig.1–The epicenter and fault area of 2010 Maule (Chile) Earthquake, seismic gap and largest earthquakes and the estimated rupture areas from 1906 to 2010 along the Chilean Coasts (Compiled from those of Kelleher, 1972; Beck, 1998; Lorito et al., 2011).

Materials and Methods

The main factor which determines the initial size and height of a tsunami is the amount of vertical sea floor deformation. Earthquake induced tsunamis are extremely long and rapidly moving ocean waves caused by a major dislocation of the ocean floor²⁴ which may be more than one hundred kilometers wavelengths from one wave crest to another offshore. It is

because of their long wavelengths that tsunamis behave as shallow-water waves. A wave is characterized as a shallow-water wave when the ratio between the water depth and its wavelength gets very small.

The shallow water waves are sea surface gravity waves which propagate over the sea with the wavelength much larger than the depth of the sea^{25,26,27}. Tsunami heights and arrival times could be estimated employing propagation models based on the long wave equations and the long wave equations describe the evolution of incompressible flow, neglecting density change along the depth. Therefore, tsunami waves can be described by shallow water models²⁸ and tsunami numerical models might be based on incompressible shallow water equations derived from the principles of conservation of mass and conservation of momentum^{29,30}. The finite difference, finite element or finite volume methods are often used to the form of the shallow water equations in the context of tsunami modeling^{31,32,33}. For the tsunami simulations presented herein, the SWAN (Simulating Waves Near-Shore) code^{34,35} is used to solve incompressible shallow water equations with a finite difference scheme in time and space including Coriolis and frictional effects. The model uses finite difference scheme in time which includes Coriolis and frictional effects. The set of equations to be solved are:

$$u_t + \frac{1}{\cos(\varphi)} + uu_x + vv_y + \frac{g}{\cos(\varphi)} + \eta_x = fv - \frac{g|U|v}{C^2(D+\eta)} \quad (1)$$

$$v_t + \frac{1}{\cos(\varphi)} + uv_x + vv_y + g\eta_y = -fu - \frac{g|U|v}{C^2(D+\eta)} \quad (2)$$

$$u_t + \frac{1}{\cos(\varphi)} \{[(\eta+D)u]_x + [(\eta+D)v\cos(\varphi)]_y\} = 0 \quad (3)$$

where φ is the latitude, u and v are the x and y components of the velocity U , g is the gravitational acceleration, t is the time, η is the wave height above the mean water level, f is the Coriolis parameter, C is the coefficient for bottom stress, D is the depth, and indexes refer to partial derivatives. The finite difference method is also employed by many well-known models, such as COMCOT²⁸, TUNAMI-N2^{36,37} and MOST³⁸.

As mentioned above, it is a need to compute the major dislocation of the ocean floor in the rupture area for tsunami propagation purposes. The aftershock distribution provides a first-order indication of the main shock rupture area. The aftershock distribution suggests a rupture length of 550 km³⁹. The W-Phase Inversion⁴⁰ yields a

solution with $M_0 = 2.0 \times 10^{22}$ Nm, with centroid location of 35.95°S , 72.75°W , a centroid time of 61.4 s, and a best-fitting fault plane having strike 16° , dip 14° rake 104° for the nodal plane 1 and strike 181° , dip 71° rake 86° for the nodal plane 2⁴¹. The W-Phase solution indicates landward dip on fault with northward displacement which is consistent with the tectonic setting and pattern of aftershocks. It is not possible to determine solely from a focal mechanism which of the nodal planes is in fact the main fault plane⁴². Thus, by taking into account the known tectonic features of the subduction in the region, the nodal plane 1 was chosen as the main nodal plane. The chosen nodal plane shows megathrust faulting which is the plate bounding thrust fault that accommodates between the subducting Nazca plate and the overriding South American plate. Although the aftershock distributions and focal mechanism solutions are used to reveal the rupture area and rupture character of the earthquake, it could not be understand multiple fault segments of variable local slip, rake angle and several other parameters by using only focal mechanism solutions.

Slip distribution of the 2010 Maule earthquake from the inversion of tsunami, geodetic and broadband teleseismic data show that megathrust slip occurred between 34°S , and 38°S ^{13,22,39,43,44,45}. Rupture extends bilaterally with an irregular slip distribution that initially is concentrated down-dip from the 35 km deep hypocenter, then spread bilaterally up-dip and off shore, with two strong slip patches in the south and north²². The concentration of slip to the north of the epicenter in the finite fault model of Lay et al. (2010) is consistent with the preliminary finite fault model of USGS⁴⁴ based on teleseismic signals (Fig. 2). In agreement with slip models, significant vertical co-seismic displacement in coastal areas between 1.0 m and 2.5 m occurred between 34°S , and 38°S ⁴⁶. After the 2010 Maule earthquake, a field survey was started by researchers from the various Universities of Chile to present the nature, geometry and kinematics of the co-seismic surface ruptures of the earthquake³⁹. They have identified two main fracture types according to their geometry and kinematics regardless of their origin, which are addressed separately: (1) Extensional-transensional, and (2) Compressional-transpressional. Their results show that all studied fractures are co-seismic and most of the co-seismic deformation can be explained by elastic rebound of the upper plate³⁹.

The initial sea surface displacement coincides with the seafloor displacement. Then, the

approach is based on solving the hydrodynamic equations with initial conditions at the ocean floor corresponding to a static displacement caused by the earthquake source⁴⁷. This approach is a conventional approach and provides adequate solution as shown in the existing literature^{24,26,42,48,49,50,51,52,53,54,55}.

The static displacement caused by the earthquake source, assumed to be responsible for the initial water surface deformation giving rise to the tsunami, was computed using the dislocation algorithm⁵⁶. This algorithm uses a slip amount and a reference conventional position of the fault that is translated from the epicenter, magnitude, depth to fault top, strike, dip and rake of the fault. The epicenter and the magnitude of the earthquake can be measured relatively, accurately and quickly after an earthquake occurs, however most of the other fault plane parameters can be difficult to determine and may remain unknown⁵⁷. It is possible to determine the source mechanism solutions and rupture models which indicate several properties of the causative faults named strike, dip and rake, slip distributions when numerous data become available as soon as the body and surface waves propagate to seismological stations.

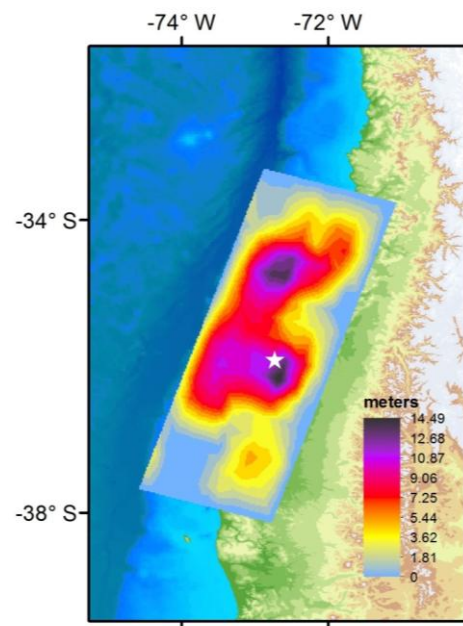


Fig.2–Surface projection of the slip distribution of the finite fault model superimposed on GEBCO30 bathymetry (GEBCO-BODC 2012)

The large rupture and duration of the mainshock of the Maule (Chile) earthquake make necessary to limit the source and rupture analysis to very long periods. The input parameters selection for the tsunami analysis presented here

were based on the rapid analysis of W-Phase source mechanism⁴¹ and finite faulting using seismic data reported by the United States Geological Survey⁴⁴ right after the event occurred based on static and seismic data inversion algorithm⁵⁸. These two analyses were indicated as uniform slip model (USM) and non-uniform slip model (NSM) in this study. The USM assumes that the slip is distributed uniformly over the entire single rectangular rupture area. The NSM assumes that the earthquake ruptures heterogeneously and the slip is distributed non-uniformly along the fault plane. Both models further assume that the sea surface follows the seafloor deformation instantaneously. By assuming the first fault plane model named USM, the vertical co-seismic displacement of the sea bottom was calculated by using earthquake parameters and fault mechanism solutions for nodal plane 1 (strike 16°, dip 14° rake 104°) provided by the W-Phase inversion from USGS⁴¹. The geometry of the fault plane for USM was adopted from a relation between fault rupture length-magnitude and fault rupture width-magnitude for the subduction dip-slip categories⁵⁹:

$$\text{Log}L = 0.55M - 2.19 \quad (4)$$

and

$$\text{Log}W = 0.31M - 0.63 \quad (5)$$

where L , W and M are fault length (km), width (km) and moment magnitude, respectively. The top of the fault was calculated as follows:

$$\text{TOF} = h - ((\text{Sin} \delta)d) \quad (6)$$

where TOF is top of the fault in km, h is the depth of earthquake (hypocenter), δ is dip angle and d is the half of the width of fault plane. The hypocentral depth estimates adopted for the initiation of the earthquake is 35 km¹.

The W-Phase solution used for creating USM considers only the focal geometry parameters (strike, dip, rake) and the scalar moment, but not the slip distribution along the fault. Therefore, the corresponding average fault slip was determined from the seismic moment M_0 and the total fault area equations^{60,61}.

$$M_0 = \mu SLW \quad (7)$$

$$M_w = \frac{2}{3} \log_{10} M_0 - 10.7 \quad (8)$$

where μ is the rigidity of earth crust, S is the amount of average slip motion (slip) and L is the length of the fault plane and W is the width of the fault plane and M_w is the moment magnitude of an earthquake. In this study, a typical value of

$4.0 \times 10^{11} \text{ dyn.cm}^{-2}$ was used for the crustal rigidity of the Pacific Rim regions⁶². Table 1 presents the source parameters applied to determine the shape of the earthquake's vertical displacement and evaluated for the tsunami simulation of the Maule (Chile) earthquake due to the USM. The maximum vertical dislocation of sea floor, in other words, the maximum sea surface response was calculated 3.50 m for the USM Modeled initial surface elevations from USM, cross-section and 3D view of the calculated seafloor deformation are displayed in Fig. 3.

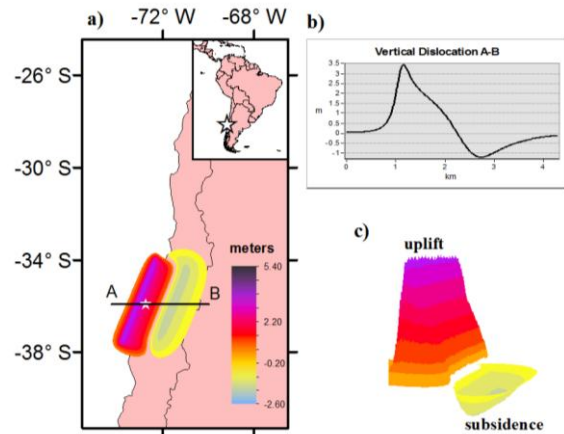


Fig.3-(a) Initial surface elevations for the uniform slip model model, (b), Cross-section of A-B due to the calculated seafloor deformation, (c) 3D view of the calculated deformation along the strike of the fault.

By assuming the second fault plane model named NSM, the vertical co-seismic displacement of the sea bottom was identified by using the finite fault model constructed through inversion algorithm of globally distributed teleseismic wave data¹. This algorithm executes the waveform inversions and provides fast and accurate coseismic slip distributions for large earthquakes immediately after the earthquake. This algorithm was also developed for real-time finite fault inversion systems to quickly evaluate the catastrophic tragedies caused by large shallow earthquakes in regional and teleseismic distances. The fault plane of the earthquake from this algorithm was defined using the W-phase moment tensor solution adjusted to match the local dip of the subducting slab⁴⁴. The using of W-Phase suggests that fast slip inversions may be carried out relying purely on W-phase records. However, it should be noted that the estimation of finite fault earthquake source models is an inherently underdetermined problem: there is no unique solution to the inverse problem of determining the rupture history at depth as a function of time and space when the data are limited to observations at the Earth's surface⁶³. The adopted finite fault

model⁴⁴ assumes that the earthquake ruptures heterogeneously and the slip is distributed non-uniformly along the fault plane. The use of the finite fault model provides more detailed information than conventional models on spatial

displacements in the source areas and avoids uncertainties in source extent^{64,65}.

Table 1- Fault parameters of the USM used for the numerical simulation

*M ₀ (dyne cm)	*Lat (°)	*Lon (°)	Depth (km)	Strike (°)	Dip (°)	Rake (°)	Length (km)	Width (km)	TOF (km)	S (m)
2.0 × 10 ²²	35.909 S	72.733 W	35	16	14	104	447	125	19.4	9.0

By carrying out the finite fault model constructed through inversion of globally distributed teleseismic wave data, the vertical co-seismic displacement of the sea bottom was identified. For this purpose, it was assumed that the sea surface followed the seafloor deformation instantaneously. The finite fault model indicated that the event ruptured a fault up to 540 km long, 200 km wide, and involved peak slip of 14.62 m. This fault model consists in 180 subfaults, 30 km × 20 km each. The slip concentrates around the hypocenter and north of hypocenter (Fig. 2). The resulting co-seismic vertical bottom displacement was calculated by assuming superposition of 180 subfaults. The maximum vertical dislocation of sea floor, in other words, the maximum sea surface response was calculated in 5.41m. Modeled initial surface elevations, cross-section and 3D view of the calculated seafloor deformation are displayed in Fig. 4.

two parts as A and B. First one covers 2.0-8.0°S and 95.0-105.0°E, second one covers 2.0-15.0°S and 92.0-111.0°E. At the computation domain A, 0.5 arc min grid was used to calculate tsunami height. At the computation domain B, 2.0 arc min grid was used. The calculations were performed using re-sampled values from the General Bathymetry Chart of the Ocean (GEBCO) 30 arc-seconds grid data (GEBCO-BODC 2012) for the computation domains. The calculation times for the tsunami propagation in the computation domain A and B is 6.0 and 3.0 hours respectively. Time steps were adjusted for satisfying the CFL (Courant–Friedrichs–Lewy) stability condition. The value of the Manning friction coefficient is assumed to be equal to 0.025 proposed for shallow water area or natural beach⁶⁶. The maps of maximum tsunami heights were shown in Figs. 5a,b and 6a,b due to the USMs and NSMs in 0.5' and 2.0' calculated grid domains.

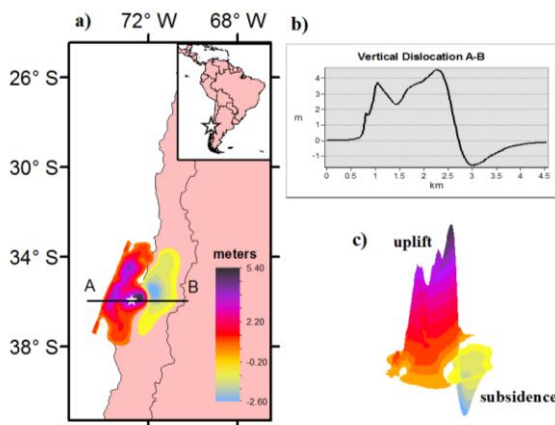


Fig.4–(a) Initial surface elevations for the finite fault model, (b), Cross-section of A-B due to the calculated seafloor deformation, (c) 3D view of the calculated deformation along the strike of the fault.

Results

The vertical dislocations, obtained above, were used as an initial height of the hydrodynamic computation on the wave simulation model SWAN. The computation domains were set in

Snapshots of tsunami wave propagations at 10 min, 30 min, 60 min, 90 min and computed water surface fluctuations within the limitations of the bathymetric grid size are plotted in Fig. 7a,b,c,d and Fig. 8a,b,c,d for the USMs and NSMs. The figures show that the most of the tsunami’s energy travels perpendicular to the strike of the fault segment. The selected locations affected by tsunami in the coastal areas of Chile with estimated maximum heights, arrival times of the maximum heights, and the first wave arrival times are displayed in Table 2 and Table 3. The comparisons of two different bathymetry cell size calculations were done by using the Green functions of wave propagation give by

$$H_c = H_0 \left(\frac{D_0}{D_i} \right)^{0.25} \quad (9)$$

where H_c is the wave heights at shore line, H₀ is the heights at the nearest calculated point, D_i is water depth at any shoreward point, and D₀ is water depth at a source point in meter⁶⁷. Accordingly, the wave heights at the shoreline were calculated by selecting the depth

corresponding to the smaller grid size close to the point that we chose as a residential area. It can be seen that the heterogeneities of the slip distribution within the fault plane are significant for the simulation of the tsunamis, especially in near field. In terms of tsunami impact, the parent fault slip heterogeneity usually determines a high variability of run-up and inundation on the near-field coasts, which further complicates the Tsunami Early Warning (TEW) problem. The variability in local tsunami run-up scaling can be ascribed to tsunami source parameters that are independent of seismic moment: variations in the water depth in the source region, the combination of higher slip and lower shear modulus at shallow depth, and rupture complexity in the form of heterogeneous slip distribution patterns⁶⁸. Before comparing the simulation results with the available DART and tide gauge waveforms, herein, the arrival times and maximum heights were compared with the observed data corresponding to several locations in the simulations, available from the National Geophysical Data Center (NGDC) web site⁶⁹. According to the NGDC⁶⁹, the waves reached Valparaiso, Coquimbo, Caldera and Ancud in 34 min, 2h 14 min, 2h 9 min, and 2h 4 min with 2.61 m, 1.32 m, 0.45 m and 0.62 m wave height respectively.

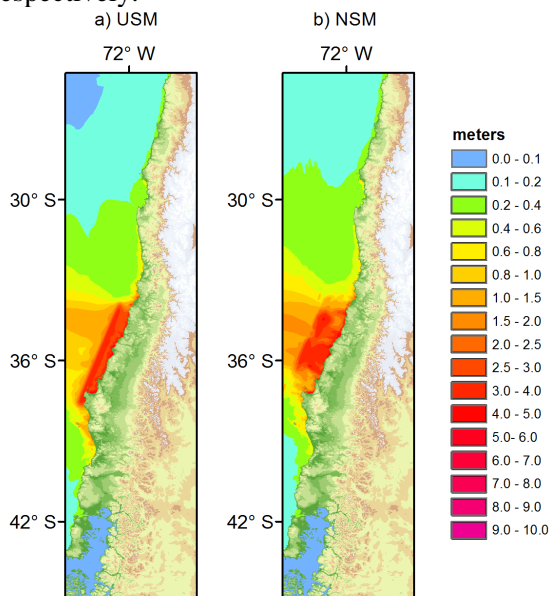


Fig.5–Maximum tsunami heights obtained from (a) uniform slip model and (b) finite fault model for computation domain A with 0.5 arc min calculation grid.

The USM (0.5') and the NSM (0.5') provide lower maximum heights when comparing to the observed waves in Valparaiso and the arrival times of maximum heights are nearly the same. In Coquimbo, the NSM (0.5') provides nearly the same maximum height with the observed

one. However, the arrival time of the maximum height is much more earlier than the observed one. In Caldera, The USM (0.5') and the NSM (0.5') provides almost the same maximum heights when comparing to the observed one. In Ancud, The USM (0.5') and the NSM (0.5') provide lower maximum heights and earlier arrival times.

In Coquimbo, the model provides nearly the same maximum height as the observed one. However, the arrival time of the maximum height is much earlier than the observed one.

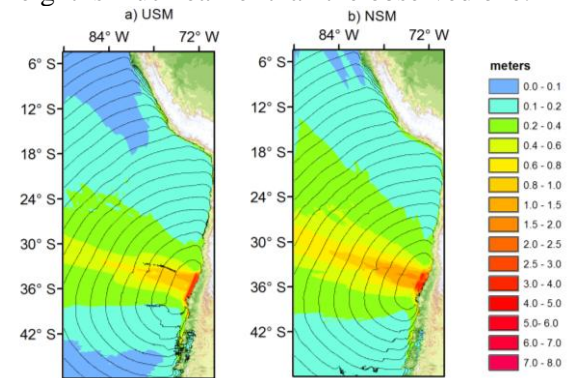


Fig.6–Maximum tsunami heights and arrival times in 15 minutes obtained from (a) uniform slip model and (b) finite fault model for computation domain B with 2.0 arc min calculation grid.

In Caldera, the model provides almost the same maximum heights when comparing to the observed one. In Ancud, the model provides lower maximum heights and earlier arrival times. This could be from geomorphologic and bathymetric local conditions, subduction geometry, absorption tsunamigenic efficiency, tsunami energy trapping and ducting which should be investigated further in the region, besides potential complexities induced by the main shock⁷⁰.

In order to adequately evaluate the results of the numerical simulation for the finite fault source model, comparisons were made between the actual observation data and calculated simulations. The observation data were recorded instrumentally at shore-based tide gauges and DART buoys⁷¹. Here, one DART buoy named 32412 and six tide gauges named Caldera, Coquimbo, Talcahuano, Corral, Ancud, San Felix were adopted for comparing the model results with the observation data. Tide gauges were installed along the Chilean coasts by Hydrographic and Oceanographic Service of Chile for National Warning System of tidal waves. The adopted DART buoy is operated by NOAA's Pacific Tsunami Warning Center in real time tsunami detection system.

DART station consists of a surface buoy and a seafloor bottom pressure recorder (BPR) package that detects pressure changes caused by tsunamis. Fig. 9 shows the locations of DART buoy and tide gauges adopted in this study with bathymetry of the Pacific Ocean around Peru–Chile Trench. A and B computation domains were used to compare tide gauge measurements and far distant sea level measurement as the DART 32412 respectively. Tsunami Analysis Tool (TAT)⁷² was used to visualize and compare tsunami propagation, tsunami travel time and maximum heights with the records of wave gauges. TAT allows a comparison of the calculated value with the available sea level measurements downloaded from

Intergovernmental Oceanographic Commission (IOC) and NOAA (National Oceanic and Atmospheric Administration) web sources^{42,72}. The time series of tsunami heights from the USM and NSM at the locations of Caldera, Coquimbo, Talcahuano, Corral, Ancud, San Felix and DART 32412 are shown in Fig. 10. For the Caldera tide gauge, the numerical models tend to give estimations that are very close to the measured data for the first recorded peak of the tsunami. The NSM provides earlier arrival times than the observed one. Both models do not match very well for the trailing waves. By comparing the simulated and observed waveforms in Coquimbo, the first and second waves almost match with the observed one.

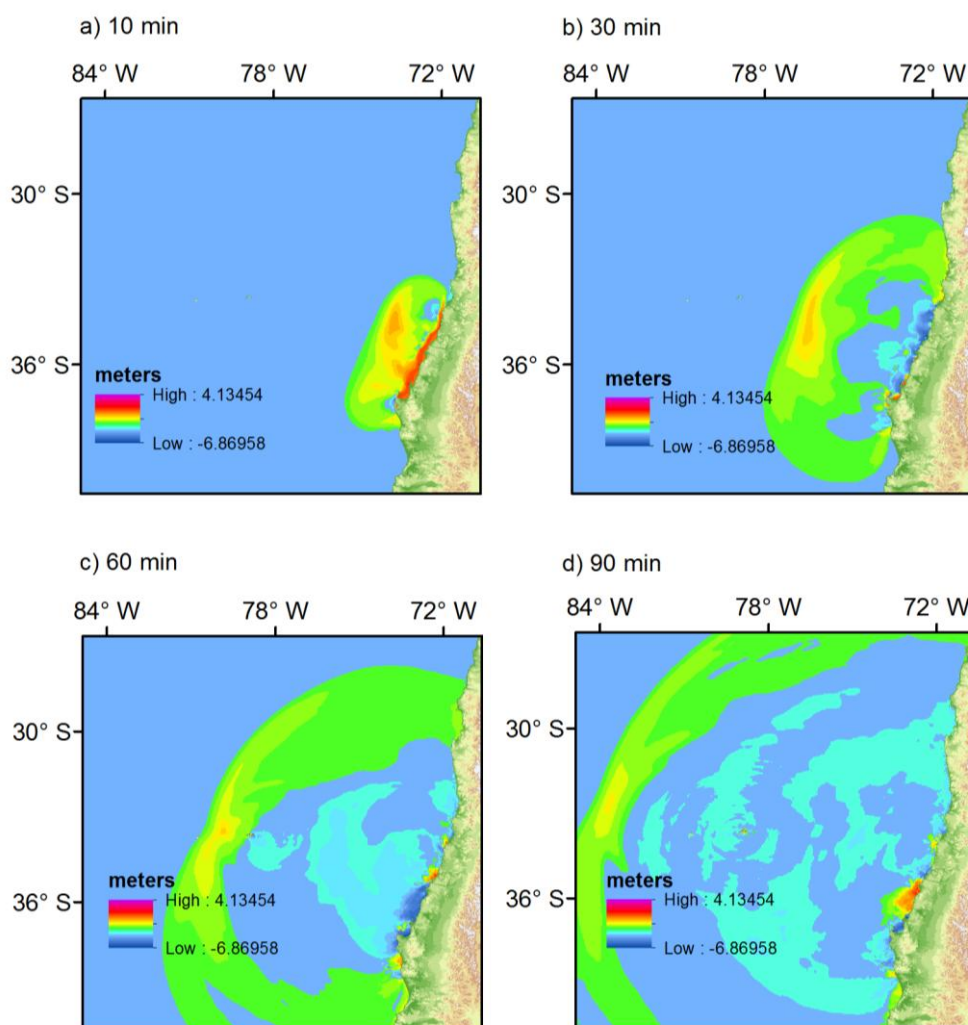


Fig.7–Snapshots of sea states at different time steps (t=10, 30, 50, 70, 90 min) from the uniform slip model in 2.0 arc min calculation domain.

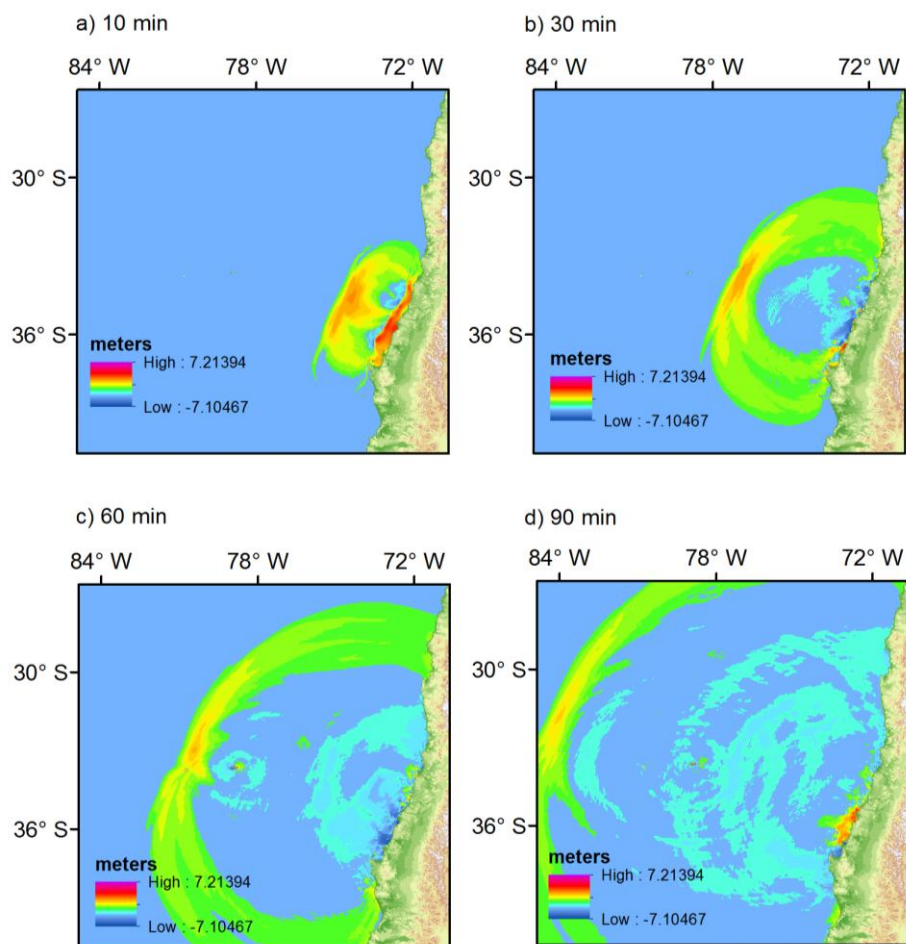


Fig.8–Snapshots of sea states at different time steps ($t=10, 30, 50, 70, 90$ min) from the finite fault model in 2.0 arc min calculation domain.

Table 2–Maximum heights according to the different slip models and calculation grids for the selected locations.

Location	Lat	Lon	USM (0.5')	NSM (0.5')	USM (2.0')	NSM (2.0')
			Max. Height (m)	Max. Height (m)	Max. Height (m)	Max. Height (m)
Lota	-37.09	-73.16	5.9	4.3	4.8	3.3
Coronel	-37.03	-73.15	5.2	3.6	6.2	3.8
Talcahuano	-36.75	-73.13	4.3	4.8	2.5	0.8
Tome	-36.61	-72.96	3.6	3.0	4.3	3.6
Constitucion	-35.32	-72.41	6.4	5.4	3.5	3.5
San Antonio	-33.60	-71.61	3.3	4.7	2.7	3.1
Llolleo	-33.62	-71.61	3.3	4.7	2.7	3.1
Quintero	-32.78	-71.54	1.7	1.9	1.1	0.8
Valparaiso	-33.02	-71.55	1.4	1.1	1.1	0.8
Concon	-32.94	-71.52	2.2	2.5	0.9	1.1
Los Vilos	-31.92	-71.51	1.4	1.2	1.0	0.8
Coquimbo	-29.97	-71.33	0.9	1.4	0.6	0.8
La Serena	-29.9	-71.24	0.9	1.0	0.4	0.5
Caldera	-27.08	-70.81	0.4	0.5	0.2	0.3
Chanaral	-26.34	-70.61	0.6	0.8	0.6	0.8
Taltal	-25.40	-70.48	0.4	0.7	0.3	0.3
Ancud	-41.86	-73.83	0.4	0.4	0.8	0.9

Table 3–First and maximum height arrival times according to the different slip models and calculation grids for the selected locations.

	Lat	Lon	USM (0.5°)		NSM (0.5°)		USM (2.0°)		NSM (2.0°)	
			*FWAT	*MHAT	*FWAT	*MHAT	*FWAT	*MHAT	*FWAT	*MHAT
Quintero	-32.78	-71.54	00:19	01:15	00:13	01:58	00:17	00:31	00:11	02:23
Valparaiso	-33.02	-71.55	00:21	00:31	00:15	00:33	00:19	00:35	00:13	00:34
Concon	-32.94	-71.52	00:21	00:38	00:15	01:50	00:19	00:35	00:13	00:34
Los Vilos	-31.92	-71.51	00:26	00:40	00:21	00:39	00:24	00:41	00:19	00:39
Coquimbo	-29.97	-71.33	00:45	01:07	00:41	01:34	00:42	01:17	00:39	01:52
La Serena	-29.90	-71.24	00:49	01:07	00:45	01:04	00:45	01:13	00:42	01:52
Caldera	-27.08	-70.81	01:11	01:31	01:07	01:27	01:10	05:47	01:06	01:36
Ancud	-41.86	-73.83	01:41	02:37	01:48	02:43	01:11	03:52	01:24	03:52
Chanaral	-26.34	-70.61	01:23	01:41	01:20	02:06	01:18	01:47	01:15	03:01
Taltal	-25.4	-70.48	01:26	01:50	01:22	02:56	01:25	01:46	01:23	01:42

*FWAT, First wave arrival time (hours: minute)

**MHAT Maximum height arrival time (hours: minute)

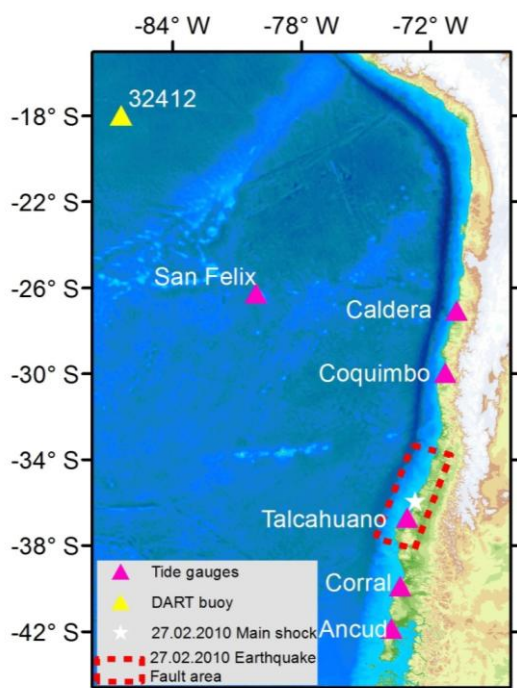


Fig.9–Location of the DART buoy and tide gauges.

The NSM provides higher waves than those of USM. The comparison is even worse for the trailing waves. For the Talcahuano tide gauge, the USM and NSM models exhibited abrupt positive leading wave while the observation remains constant in the origin time of the earthquake. This means that this station is in the uplift area of the seafloor. Although the time series of the simulated waves from both models are earlier, the amplitudes and periods of the waves are in good agreement with the records of Talcahuano tide gauge. Talcahuano is a port city in the Biobío Region of Chile which was one of the mostly affected cities from tsunami with about 7 m run-

up height and 340 m inundation distance⁶⁴. By comparing the simulated and observed waveforms in Corral, the arrival times of the simulated waves are in good agreement with the observed ones. However the heights and the waveforms of the trailing waves do not match with the observed one. The NSM provides lower heights than the USM and measured waves. For Ancud, the comparison is worse. The arrival times and the periods of the waves are totally missed by the numerical results. However, the simulated maximum heights match well with the observed Ancud tide gauge record. The latest compared measurement is the data recorded by San Felix tide gauge station. It is located in Juan Fernandez Island which is a volcanic island and seamount chain on the Nazca Plate. The numerical simulations are compared well with the measured leading wave heights and arrival times in the San Felix tide gauge.

Finally, the simulations from from USM and NSM, compared with the DART 32412 records, produce similar tsunami amplitudes apparently close to the observed ones (Fig.11). It should be noted that the exact reproduction of the tidal gauges is not easy because the local conditions where the gauge is installed may strongly influence their response. The comparisons between observed tidal records and predicted waveforms may not be in good agreement compared to those of DART records. Because, the characteristics of the ocean bottom topography is particularly important over the continental shelves, where the amplitude of the waves is amplified by the shoaling of the bottom topography. Hence, correctly and finer reproduced bathymetry requires for a correct estimation of the tsunami heights on coastal areas where the tide gauges installed. Additionally, the

use of a more finer grid calculations could allow predicting higher wave heights because the points become more representative of the real depth⁴². In

this study, the above mentioned Green function approach was used to mitigate these differences.

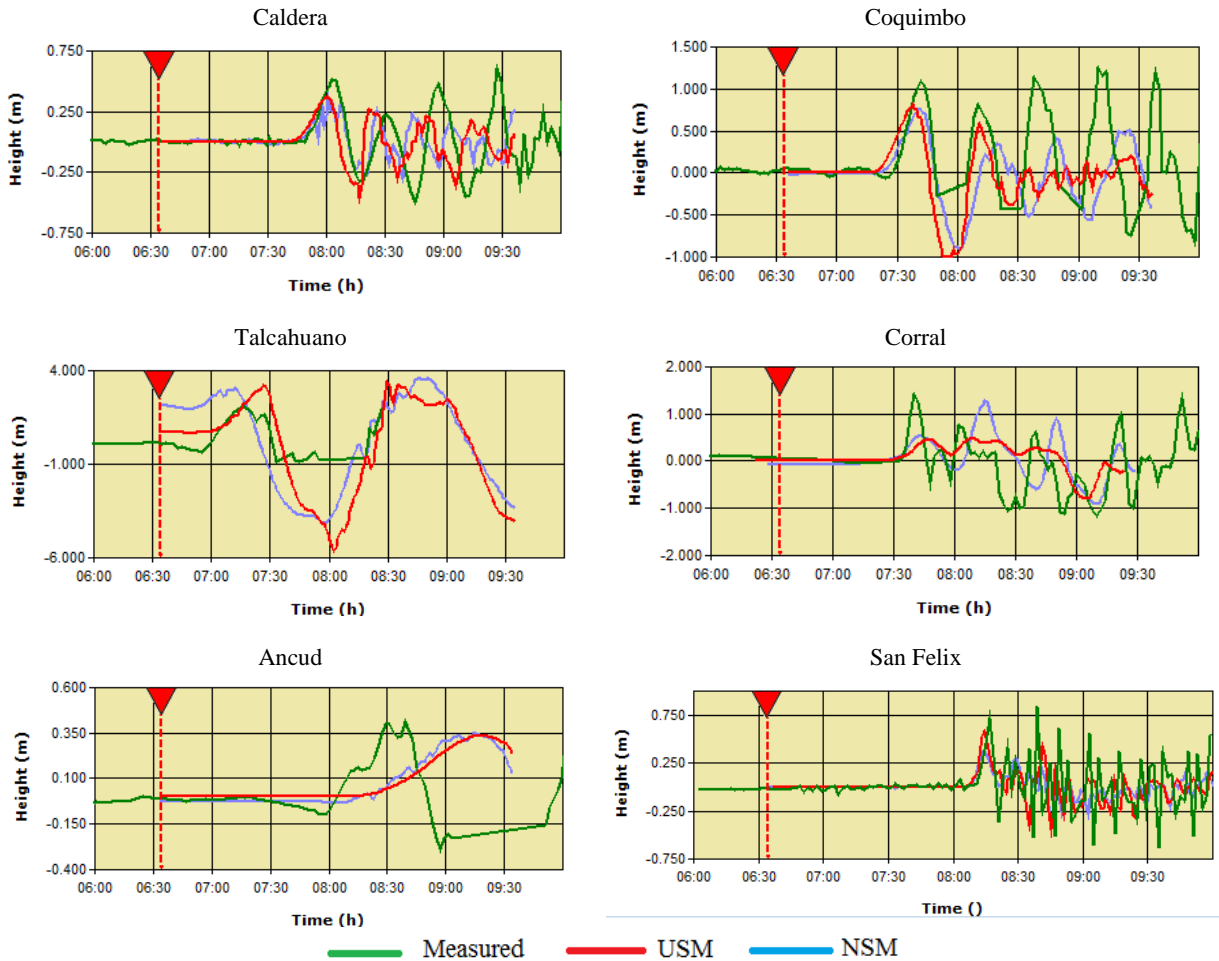


Fig.10–Comparison of the predicted tsunami waves from the finite fault model with observed tide gauge records.

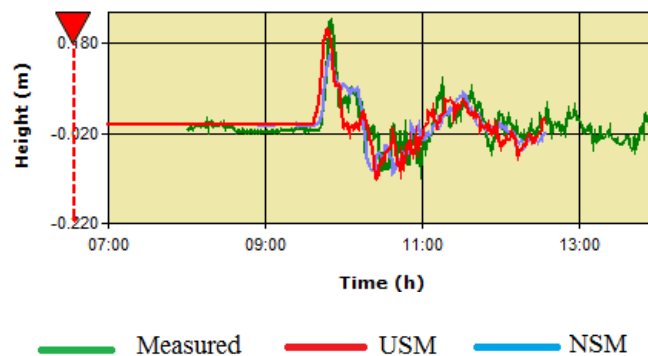


Fig.11–Comparison of the predicted tsunami waves from the finite fault model with observed 32412 DART buoy record.

Discussion

The 27 February 2010 Maule (Chile) earthquake, with the magnitude of M_w 8.8, produced much lower tsunami heights in several areas of Pacific Ocean compared to those of 1960 Great Chile Earthquake. The main reason for this is the lower

magnitude of 2010 Maule (Chile) earthquake compared with the 1960 earthquake with a magnitude of 9.0. On the other hand, it was expected that the far field tsunami impact would have been somewhat larger due to the magnitude of the earthquake. However, the measured

tsunami heights was not as severe as anticipated in the far field. The observed run-ups along Chile's mainland both at local and regional scales showed that the coastal cities Talcahuano, Constitucion, Lota, Coronel, Dichato, Concepcion were hardest hit. Numerical simulations of the tsunami from the USMs and NSMs were carried out to clarify the impact of near field tsunami along the coastline of Chile. Numerical tsunami simulations were computed from a simplified elastic dislocation representation of the earthquake source. The proposed USM involves the rupture area with a 447 m length and 125 m width and the average slip as 8.26 m. The adopted NSM indicates that the event ruptured a fault up to 540 km length, 200 km width, and involved peak slip of 14.62 m. After employing the USM and NSM source models, the maximum vertical sea floor dislocations were calculated as 3.49 m and 5.41 m of uplift and 1.19 m and 2.60 m of subsidence respectively. These are the reasonable values to induce and propagate tsunamis along the Pacific Ocean. The modeling of the vertical variations of the earthquake from the finite fault model indicated that the wide leading uplift occurred close to the coast both on the sea floor and onshore. However, the rest of other part of the rupture zone continued to land areas with uplift and subsidence. A wide subsidence area accumulated inland site. From the point of this approach, some of the releasing energy of the earthquake might be absorbed by the movement of the uplift and subsidence on land, and not all of the energy was transferred to generate the tsunami wave⁷³. This situation could be one of a reason that the tsunami was not severe in the far field. The modeled uplift, subsidence, and the comparisons of the simulated waves with observed records confirm this approach as proposed by previous studies^{73,74}.

Conclusion

Although the location of the epicenter is in a clearly identified seismic gap area within the subduction zone, there was small area of slip south of the epicenter that was in the proposed seismic gap¹². The pattern of largest slips was located in the north of the gap. This means that the gap may not be filled and probably endures. In this sense, the estimated simulations and the concluding remarks from this study can help to identify the vertical dislocations from the similar earthquakes and possible impact of the tsunamis in the region for the preservation of the loss of lives and cities.

Acknowledgements

Author would also like to express deep appreciation to the Scientific and Technological Research Council of Turkey (TUBITAK) for the financial support.

References

- 1 U.S. Geological Survey (USGS), Earthquake Hazards Program, Earthquake details, Magnitude 8.8 Offshore Bio-Bio, Chile, <http://earthquake.usgs.gov/earthquakes/> (last access on 21 July 2012).
- 2 Gutscher, M.A., Andean subduction styles and their effect on thermal structure and interplate coupling, *J. S. Am. Earth Sci.*, 15(2002) 3-10.
- 3 Uyeda, S., and Kanamori, H., Back-Arc Opening and the Mode of Subduction, *J. Geophys. Res.* 84(1979) 1049-1061.
- 4 Lomnitz, C., Major earthquakes of Chile: a historical survey, 1535-1960, *Seismol. Res. Lett.*, 75(2004) 368-378.
- 5 Lomnitz, C., Major earthquakes and tsunamis in Chile during the period 1535 to 1955, *Int. J. Earth Sci.*, 59(1970) 938-960.
- 6 Kelleher, J., Rupture zones of large South American earthquakes and some predictions, *J. Geophys. Res.*, 77(1972), 2089-2103.
- 7 Comte, D., Eisenberg, A., Lorca, E., Pardo, M., Ponce, L., The central Chile earthquake of 3 March 1985: a repeat of previous great earthquakes in the region, *Science* 233(1986) 449-453.
- 8 Cisternas, M., Torrejón, F., Gorigoitia, N., Amending and complicating Chile's seismic catalog with the Santiago earthquake of 7 August 1580, *J. S. Am. Earth Sci.*, 33(2012) 102-109.
- 9 Watt, S.F.L., Pyle, D.M., Mather, T.A., The influence of great earthquakes on volcanic eruption rate along the Chilean subduction zone, *Earth Planet Sc. Lett.*, 277(2009), 399-407.
- 10 Lomnitz, C., Tectonic feedback and the earthquake cycle, *Pure Appl. Geophys.*, 123(1985) 667-682.
- 11 Klotz, J., Khazaradze, G., Angermann, D., Reigber, C., Perdomo, R., and Cifuentes, O., Earthquake cycle dominates contemporary crustal deformation in Central and Southern Andes, *Earth Planet Sc. Lett.*, 193(2001) 437-446.
- 12 DeMets, C., Gordon, R., Argus, D., and Stein, S., Effect of recent revision to the geomagnetic reversal time scale on estimates of current plate motion, *Geophys. Res. Lett.* 21(1994) 2191-2194.
- 13 Lorito, S., Romano, F., Atzori, S., Tong, X., Avallone, A., McCloskey, J., Cocco, M., Boschi, E., and Piatanesi A., 2011, Limited overlap between the seismic gap and coseismic slip of the great 2010 Chile earthquake, *Nat. Geosci.*, 4(2010) 173-177.
- 14 Leyton, F., Ruiz, S., and Sepulveda, S. A., Preliminary re-evaluation of probabilistic seismic hazard assessment in Chile: from Arica to Taitao Peninsula, *Adv. Geosci.*, 22(2009) 147-153.
- 15 Lemoine, A., Madariaga, R., Campos, J., Slab-pull and slab-push earthquakes in the Mexican, Chilean and Peruvian subduction zones, *Phys., Earth Planet In.*, 132(2002) 157-175.
- 16 Barrientos, S., Is the Pichilemu Talcahuano (Chile) a seismic gap, *Seismol. Res. Lett.*, 61(1990) 43-48.
- 17 Campos, J., Hatzfeld, D., Madariaga, R., López, G., Kausel, E., Zollo, A., Iannaccone, G., Fromm, R.,

- Barrientos, S., and Lyon-Caen, H., 2002, A seismological study of the 1835 seismic gap in south-central Chile, *Phys. Earth Planet. Inter.*, 132(2002) 177–195.
- 18 Carayannis, G.P., The Earthquake And Tsunami Of 27 February 2010 In Chile –Evaluation of Source Mechanism And of Near And Far-Field Tsunami Effects, *Sci. Tsu. Hazards*, 29(2010) 96-126.
- 19 Moreno, M., Rosenau, M., and Oncken, O., Maule earthquake slip correlates with pre-seismic locking of Andean subduction zone, *Nature*, 467(2010) 198-204.
- 20 Haberland, C., Rietbrock, A., Lange, D., Bataille, K., and Dahm, T., Structure of the seismogenic zone of the southcentral Chilean margin revealed by local earthquake traveltime tomography, *J. Geophys. Res.* 114(2009) B01317
- 21 Ruegg, J. C., Rudloff, A., Vigny, C., Madariaga, R., Chabalier, J.B., Campos, J., Kausel, E., Barrientos, S and Dimitrov, D., Interseismic strain accumulation measured by GPS in the seismic gap between Constitución and Concepción in Chile, *Phys. Earth Planet. Inter.* 175(2009) 78–85..
- 22 Lay, T., Ammon, C.J., Kanamori, H., Koper, K.D., Sufri, O., and Hutko, A.R., Teleseismic inversion for rupture process of the 27 February 2010 Chile (Mw 8.8) earthquake, *Geophys. Res. Lett.*, 37(2010), L13301.
- 23 Fritz, H.M., Petroff, C.M., Catala´ N, P.A., Cienfuegos, R., Winckler, P., Kalligeris, N., Weiss, R., Barrientos, S.E., Meneses, G., Valderas-Bermejo, C., Ebeling, C., Papadopoulos, A., Contreras, M., Almar, R., Dominguez, J.C., and Synolakis, C.E., Field survey of the 27 February 2010 Chile tsunami, *Pure Appl. Geophys.* 168(2010) 1989–2010.
- 24 Ulutas, E., Comparison of the seafloor displacement from uniform and non-uniform slip models on tsunami simulation of the 2011 Tohoku–Oki earthquake, *J. Asian Earth Sci.*, 62(2013) 568–585.
- 25 Hebert, H., Schindele, F., Heinrich, P., Tsunami risk assessment in the Marquesas Islands (French Polynesia) through numerical modeling of generic far-field events, *Nat. Hazards Earth Syst. Sci.*, 1(2001) 233–242.
- 26 Kanoglu, U., and Synolakis, C.E., Initial value problem solution of nonlinear shallow water-wave equations, *Phys. Rev. Lett.*, 97(2006) 148501-148504.
- 27 Baran, A., *Analytical Solutions of Shallow-Water Wave Equations*, PhD Thesis, Middle East Technical University, Ankara, 2011.
- 28 Liu, P.L.-F., Woo, S.B., and Cho, Y.S., *Computer Programs for Tsunami Propagation and Inundation*, (Cornell University, Sponsored by National Science Foundation) 1998, pp. 1087.
- 29 Intergovernmental Oceanography Commission (IOC), *Numerical method of tsunami simulation with the leap frog scheme, I, shallow water theory and its difference scheme*, (Manuals and Guides of the IOC, UNESCO, Paris) 1997, pp. 12-19.
- 30 Hébert, H., Schindelé, F., Altinok, Y., Alpar, B., and Gazioglu, C., Tsunami hazard in the Marmara sea (Turkey): a numerical approach to discuss active faulting and impact on the Istanbul coastal areas, *Mar. Geol.*, 215(2005) 23–43.
- 31 Goto, C., Ogawa, Y., Shuto, N., and Imamura, N., *Numerical method of tsunami simulation with the leap-frog scheme*, (IUGG/IOC Time Project. IOC Manual) 1997, pp. 58.
- 32 Piatanesi, A., Tinti, S., Finite-element numerical simulations of tsunamis generated by earthquakes near circular islands, *Bull. Seism. Soc. Am.*, 88(1998) 609-620.
- 33 Franchello, G., Shoreline tracking and implicit source terms for a well balanced inundation model, *Int. J. Num. Meth. Fluids*, 63(2010) 1123–1146.
- 34 Mader, C., *Numerical Modeling of water waves*, (University of California Press, Berkeley, California) 1988, pp.206.
- 35 Mader, C.L., *Numerical modeling of water waves.*, (CRC, Boca Raton, ISBN 0-8493-2311-8), 2004, pp.1–274.
- 36 Imamura, F., Shuto, N., and Goto, C., Numerical simulation of the transoceanic propagation of tsunamis, paper presented at *the Sixth Congress of the Asian and Pacific Regional Division, Int. Assoc. Hydraul. Res.*, Kyoto, Japan, 1988.
- 37 Imamura, F., Yalciner, A. C., and Ozyurt, G., 2006, Tsunami Modelling Manual, available from: <http://ioc3.unesco.org/TsunamiTeacher/data/Resource/PDF/PubPriv109TMM.pdf>, last access: 25 November 2011.
- 38 Titov, V.V., and Synolakis, C.E., Extreme inundation flows during the Hokkaido-Nansei-Oki tsunami, *Geophys. Res. Lett.*, 24(1997) 1315–1318.
- 39 Arriagada, C., Arancibia, G., Cembrano, J., Martínez, F., Carrizo, D., Van Sint Jan, M., Sáez, E., González, G., Rebolledo, S., Sepúlveda, S.A., Contreras-Reyes, E., Jensen, E., Yañez, G., 2011. Nature and tectonic significance of co-seismic structures associated with the Mw 8.8 Maule earthquake, central-southern Chile forearc, *J. Struct. Geol.*, 33(2011) 891-897.
- 40 Kanamori, H., Rivera, L.A., Speeding up seismic tsunami warning, *Geophys. J. Int.*, 17(2008) 222–238.
- 41 U.S. Geological Survey (USGS), Earthquake Hazards Program, USGS WPhase Moment Solution, <http://earthquake.usgs.gov/earthquakes/eqinthenews/> (last access on 21 July 2012).
- 42 Ulutas, E., Inan, A., Annunziato, A., 2012, Web-based Tsunami Early Warning System: a case study of the 2010 Kepulauan Mentawai Earthquake and Tsunami, *Nat. Hazards Earth Syst. Sci.*, 12(2012) 1855–1871.
- 43 Delouis, B., Nocquet, J.-M., Vallée, M., Slip distribution of the February 27, 2010 Mw = 8.8 Maule earthquake, central Chile, from static and highrate GPS, InSAR, and broadband teleseismic data, *Geophys. Res. Lett.*, 37(2010) L17305.
- 44 Hayes, G., 2010, Finite Fault Model of the 27 February 2010 Magnitude 8.8 Maule (Chile) Earthquake, available from: http://earthquake.usgs.gov/earthquakes/eqinthenews/2010/us2010tfan/finite_fault.php, last access on 21 July 2012.
- 45 Tong, X., Sandwell, D., Luttrell, K., Brooks, B., Bevis, M., Shimada, M., Foster, J., Smalley Jr., R, Parra, H., Soto, J.C.B., Blanco, M., Kendrick, E., Genrich, J., Caccamise, D.J., The 2010 Maule, Chile earthquake: Downdip rupture limit revealed by space geodesy, *Geophys. Res. Lett.*, 37(2010) L24311.
- 46 Fariás, M., Vargas, G., Tassara, A., Carretier, S., Baize, S., Melnick, D., Bataille, K., 2010. Land-Level changes produced by the Mw 8.8 2010 Chilean earthquake. *Science*, 329(2010) pp.916.
- 47 Paulatto, M., Pinat, T., and Romanelli, F., Tsunami hazard scenarios in the Adriatic Sea domain, *Nat. Hazards Earth Syst. Sci.* 7(2007) 309–325.
- 48 Titov, V.V. and Synolakis, C.E., Numerical modeling of tidal wave runup *J. Waterw. Port. C. Div.*, 124(1998) 157–171.
- 49 Baptista, M.A., Miranda, J.M., Chierici, F., Zitellini, N., New study of the 1755 earthquake source based on multi-channel seismic survey data and tsunami modeling, *Nat. Hazards Earth Syst. Sci.*, 3(2003) 333–340.

- 50 Yalciner, A., Pelinovsky, E., Talipova, T., Kurkin, A., Kozelkov, A., and Zaitsev, A., Tsunamis in the Black Sea: comparison of the historical, instrumental, and numerical data. *J. Geophys. Res.*, 109(2004) C12023.
- 51 Titov, V., Rabinovich, A.B., Mofjeld, H.O., Thomson, R.E., and Gonzalez, F., The global reach of the 26 December 2004 Sumatra tsunami, *Science*, 309(2005) 2045-2048
- 52 Lorito, S., Tiberti, M. M., Basili, R., Piatanesi, A., and Valensise, G., Earthquake-generated tsunamis in the Mediterranean Sea: Scenarios of potential threats to Southern Italy, *J. Geophys. Res.* 113(2008) B01301.
- 53 Okal, E., Synolakis, C.E., and Kalligeris, N., Tsunami Simulations for Regional Sources in the South China and Adjoining Seas, *Pure Appl. Geophys.*, 168(2011)1153-1173.
- 54 Yolsal-Çevikbilen, S., and Taymaz, T., Earthquake source parameters along the Hellenic subduction zone and numerical simulations of historical tsunamis in the Eastern Mediterranean, *Tectonophysics*, 536–537(2012) 61–100.
- 55 Matias, L.M., Cunha, T., Annunziato, A., Baptista, M.A., Carrilho, F., Tsunamigenic earthquakes in the Gulf of Cadiz: fault model and recurrence, *Nat. Hazards Earth Syst. Sci.*, 13(2013) 1–13.
- 56 Okada, Y., Surface deformation due to shear and tensile faults in a half-space, *Bull. Seismol. Soc. Am.* 75(1985), 1135–1154.
- 57 Synolakis, C., Liu, P.L.-F., Carrier, G., and Yeh, H., Tsunamigenic seafloor deformations. *Science*, 278(1997) 598-600.
- 58 Ji, C., Wald, D.J., Helmberger, D.V., Source description of the 1999 Hector Mine, California earthquake; Part I: Wavelet domain inversion theory and resolution analysis, *Bull. Seism. Soc. Am.*, 92(2002) 1192-1207.
- 59 Papazachos, B.C., Scordilis, E.M., Panagiotopoulos, D.G., Papazachos, C.B., and Karakaisis, G.F., Global relations between seismic fault parameters and moment magnitude of earthquakes, *Bull. Geol. Soc. of Greece*, 36(2004) 1482-1489.
- 60 Aki, K., Generation and propagation of G waves from the Niigata earthquake of June 14, 1964. Part 2, Estimation of earthquake moment, released energy and stress-strain drop from G wave spectrum, *Bull. Seismol. Soc. Am.*, 44(1966) 73-88.
- 61 Hanks, T.C., Kanamori, H., A moment magnitude scale. *J. Geophys. Res.*, 84(1979) 2348-2350.
- 62 Johnson, J. M., Heterogeneous coupling along Alaska-Aleutians as inferred from tsunami, seismic, and geodetic inversions, *Advances in Geophysics*, 39(1999) 1–110.
- 63 Minson, S.E., Simons, M., Beck, J. L., Bayesian inversion for finite fault earthquake source models I-theory and algorithm, *Geophys. J. Int.*, 194(2013) 1701-1726.
- 64 Rabinovich, A.B., Lobkovsky, L.I., Fine, I.V., Thomson, R.E., Ivelskaya, T.N., Kulikov, E.A., Near-source observations and modeling of the Kuril Islands tsunamis of 15 November 2006 and 13 January 2007, *Adv. Geosci.*, 14(2008) 105–116.
- 65 Grilli, S.T., Harris, J.C., Tajalibakhsh, T., Kirby, J.T., Shi, F., Masterlark, T.L., and Kyriakopoulos, C., Numerical simulation of the 2011 Tohoku tsunami: Comparison with field observations and sensitivity to model parameters, paper presented at the 22nd International Offshore and Polar Engineering Conference, Rodos, Greece, 2012.
- 66 Koshimura, S., Oie, T., Yanagisawa, H., and Imamura, F., Developing Fragility Functions For Tsunami Damage Estimation Using Numerical Model and Post-Tsunami Data From Banda Aceh, Indonesia, *Coast. Eng. J.* 51 (2009) 243–273.
- 67 Geist, E.L., Local tsunamis and earthquake source parameters, *Adv. Geophys.*, 39(1997) 117-209.
- 68 Geist, E.L., Complex earthquake rupture and local tsunamis, *J. Geophys. Res.*, 107 (2002) 1-6.
- 69 National Geophysical Data Center (NGDC), Recent and significant tsunami events, <http://www.ngdc.noaa.gov/hazard/recenttsunamis.shtml>, (last access on 20 June 2012).
- 70 Vargas, G., Fariás, M., Carretier, S., Tassara, A., Baize, S., Melnick, D., Coastal uplift and tsunami effects associated to the 2010 Mw8.8 Maule earthquake in Central Chile, *Andean Geol.*, 38(2011) 219-238.
- 71 González, F. I., Bernard, E. N., Meinig, Ebel, M.C., Mofjeld, H.O., Stalin, S., The NTHMP tsunameter network, *Nat. Hazards*, 35(2005) 25–39,
- 72 Annunziato, A., Ulutas, E., and Titov, V. V., 2009, Tsunami Model Study Using JRC-SWAN and NOAA-SIFT Forecast Methods, paper presented at the International Symposium on Historical Earthquakes and Conservation of Monuments and Sites in the Eastern Mediterranean Region 500th Anniversary Year of the 1509, 2009.
- 73 Wen, R., Ren, Y., Li, X., Pan, R., Comparison of two great Chile tsunamis in 1960 and 2010 using numerical simulation, *Earthq Sci.*, 24(2011), 475–483.
- 74 Synolakis, C. E., Fritz, H. M., Petroff, C. M., Catalan, P. A., Cienfuegos, R., Winckler, P., Kalligeris, N., Weiss, R., Meneses, G., Valderas-Bermejo, C., Ebeling, C. W., Papadopoulos, A., Contreras, M., Almar, R., Dominguez, J. C., Barrientos, S. E., Observations and Modeling of the 27 February 2010 Tsunami in Chile, paper presented at American Geophysical Union Fall Meeting, San Francisco, CA, 2010